136th MEETING

ACOUSTICAL SOCIETY OF AMERICA

Calculation of Sound Scattering from Elastic Targets Using Unified FDTD Formulae

Shuozhong Wang*, Rongqing Wang**, and Zhen Fang*

**Shanghai University, Shanghai 200072, P. R. China*

***760 Research Institute, Dalian 116013, P. R. China*

Norfolk, Virginia

12-16 October 1998

Calculation of Sound Scattering from Elastic Targets Using Unified FDTD Formulae[1]

Shuozhong Wang*, Rongqing Wang**, and Zhen Fang*

**Shanghai University, Shanghai 200072, P. R. China*

***760 Research Institute, Dalian 116013, P. R. China*

Abstract

In many realistic underwater targets, both longitudinal and transverse waves exist. In order to deal with sound scattering from such objects, a set of FDTD expressions are established based on Hook's law. The expressions reduce to the previously obtained form for "liquid" objects if shear wave is absent. On the interface between the water and the solid scatterer, the boundary conditions are satisfied by introducing two compliance coefficients which are the averages of compressive compliance and shear compliance of the two media, respectively. Thus the FDTD iteration can be done in a unified manner in both media as well as on the boundary. A major advantage of the unified formulation is the potential for a significant reduction of the computation burden. The saving is achieved by using array operations to remove most of the loops. It makes the finite-difference field computation very efficient and, more importantly, suitable for the implementation of distributed parallel computing. Numerical experiment results for scattering from an aluminum bar with a complicated section and submerged in sea water are presented.

I. Introduction

Since the mid-90's, the finite-difference time-domain method has been applied to solve a number of acoustical problems. Examples include a study of underwater scattering by an object insonified by a steady-state sinusoidal plane incident wave[1,2], simulation of wave propagation in borehole environment[3], sound scattering from a rough sea surface[4,5], and implementation of transparent sources embedded in finite-difference grids[6].

In [1] and [2], the basic FDTD iterative relations and absorbing boundary conditions were established. These are suitable for numerical computations of sound scattering and target characteristics. The idea is to replace the first-order spatial and temporal derivatives in the motion equation and the equation of continuity with relevant central differences, and simulate the wave propagation in an iterative manner. Boundary conditions at the object surface are naturally satisfied during the iteration. In this way, field distributions can be obtained. Good agreement between FDTD

[1] This work was supported by the National Natural Science Foundation of China.

results and rigorous or asymptotic solutions has been demonstrated for ideally soft and rigid scattering objects.

The method was then extended to treat "fluid" objects having a finite acoustic impedance[7,8], and elastic objects in which transverse waves exist[9]. It has been shown that the FDTD formulae may be expressed in a unified fashion to cover a wide range of scattering objects, from opaque to penetrable, and from fluid to elastic.

In the FDTD field simulation, field parameters at each lattice node must be calculated at each iteration step. Based on the expressions given in the previous work, any FDTD field computation involves a prime loop for the temporal iteration, and two or three loops to cover the lattice nodes in the computation domain. This inevitably results in an enormous computation burden.

In Section II of this paper, the unified FDTD formulae are first introduced. A modification to the algorithm is then described in the next section, making the method more suitable to the study of practical scattering problems, especially in cases where the target has a complicated shape. Numerical experiments using the improved algorithm have been performed. The results are presented in Section IV. The final section concludes the paper.

II. Unified FDTD Formulation

1 Sound waves in elastic media

In an isotropic and homogeneous elastic medium, stress and strain are governed by the Hooke's law:

$$\left.\begin{aligned} T_{xx} &= \lambda(\varepsilon_{xx}+\varepsilon_{yy}+\varepsilon_{zz})+2\mu\varepsilon_{xx} = (\lambda+2\mu)\Delta-2\mu(\varepsilon_{yy}+\varepsilon_{zz}) \\ T_{yy} &= \lambda(\varepsilon_{xx}+\varepsilon_{yy}+\varepsilon_{zz})+2\mu\varepsilon_{yy} = (\lambda+2\mu)\Delta-2\mu(\varepsilon_{zz}+\varepsilon_{xx}) \\ T_{zz} &= \lambda(\varepsilon_{xx}+\varepsilon_{yy}+\varepsilon_{zz})+2\mu\varepsilon_{zz} = (\lambda+2\mu)\Delta-2\mu(\varepsilon_{xx}+\varepsilon_{yy}) \\ T_{yz} &= \mu\varepsilon_{yz} \\ T_{zx} &= \mu\varepsilon_{zx} \\ T_{xy} &= \mu\varepsilon_{xy} \end{aligned}\right\} \tag{1}$$

In these equations, T_{xx}, T_{yy} and T_{zz} are compressive stress components. T_{yz}, T_{zx}, and T_{xy} are shear stress components. ε_{xx}, ε_{yy} and ε_{yy} are compressive strains ($\Delta = \varepsilon_{xx}+\varepsilon_{yy}+\varepsilon_{zz}$); while ε_{yz}, ε_{zx} and ε_{xy} are shear strains:

$$[\mathbf{E}] = \begin{bmatrix} \varepsilon_{xx} & \varepsilon_{xy} & \varepsilon_{zx} \\ \varepsilon_{yx} & \varepsilon_{yy} & \varepsilon_{yz} \\ \varepsilon_{zx} & \varepsilon_{zy} & \varepsilon_{zz} \end{bmatrix} = \begin{bmatrix} \dfrac{\partial\xi}{\partial x} & \dfrac{\partial\eta}{\partial x}+\dfrac{\partial\xi}{\partial y} & \dfrac{\partial\xi}{\partial z}+\dfrac{\partial\zeta}{\partial x} \\ \dfrac{\partial\eta}{\partial x}+\dfrac{\partial\xi}{\partial y} & \dfrac{\partial\eta}{\partial y} & \dfrac{\partial\zeta}{\partial y}+\dfrac{\partial\eta}{\partial z} \\ \dfrac{\partial\xi}{\partial z}+\dfrac{\partial\zeta}{\partial x} & \dfrac{\partial\zeta}{\partial y}+\dfrac{\partial\eta}{\partial z} & \dfrac{\partial\zeta}{\partial z} \end{bmatrix} \tag{2}$$

where ξ, η and ζ are displacements. λ and μ are Lame constants of the medium.

Also, the stress and particle velocity are related through the Newton's second law.

$$\left.\begin{aligned}\frac{\partial T_{xx}}{\partial x}+\frac{\partial T_{xy}}{\partial y}+\frac{\partial T_{xz}}{\partial z}&=\rho\frac{\partial^2\xi}{\partial t^2}=\rho\frac{\partial v_x}{\partial t}\\ \frac{\partial T_{yx}}{\partial x}+\frac{\partial T_{yy}}{\partial y}+\frac{\partial T_{yz}}{\partial z}&=\rho\frac{\partial^2\eta}{\partial t^2}=\rho\frac{\partial v_y}{\partial t}\\ \frac{\partial T_{zx}}{\partial x}+\frac{\partial T_{zy}}{\partial y}+\frac{\partial T_{zz}}{\partial z}&=\rho\frac{\partial^2\zeta}{\partial t^2}=\rho\frac{\partial v_z}{\partial t}\end{aligned}\right\} \tag{3}$$

where $v_x = \partial\xi/\partial t$, $v_y = \partial\eta/\partial t$ and $v_z = \partial\zeta/\partial t$ are particle velocity components.

Based on these laws, and by choosing a nonstaggered lattice structure and replacing the partial derivatives in the equations with central differences, the following FDTD formulae for elastic media are obtained:

$$T_{xx}^{(n)}(i,j)=T_{xx}^{(n-2)}(i,j)+(\lambda+2\mu)\frac{\Delta t}{\delta}\left[v_x^{(n-1)}(i+1,j)-v_x^{(n-1)}(i-1,j)\right]+\lambda\frac{\Delta t}{\delta}\left[v_y^{(n-1)}(i,j+1)-v_y^{(n-1)}(i,j-1)\right] \tag{4}$$

$$T_{yy}^{(n)}(i,j)=T_{yy}^{(n-2)}(i,j)+(\lambda+2\mu)\frac{\Delta t}{\delta}\left[v_y^{(n-1)}(i,j+1)-v_y^{(n-1)}(i,j-1)\right]+\lambda\frac{\Delta t}{\delta}\left[v_x^{(n-1)}(i+1,j)-v_x^{(n-1)}(i-1,j)\right] \tag{5}$$

$$T_{xy}^{(n)}(i,j)=T_{xy}^{(n-2)}(i,j)+\mu\frac{\Delta t}{\delta}\left[v_y^{(n-1)}(i+1,j)-v_y^{(n-1)}(i-1,j)+v_x^{(n-1)}(i,j+1)-v_x^{(n-1)}(i,j-1)\right] \tag{6}$$

$$v_x^{(n)}(i,j)=v_x^{(n-2)}(i,j)+\frac{1}{\rho}\frac{\Delta t}{\delta}\left[T_{xx}^{(n-1)}(i+1,j)-T_{xx}^{(n-1)}(i-1,j)+T_{xy}^{(n-1)}(i,j+1)-T_{xy}^{(n-1)}(i,j-1)\right] \tag{7}$$

$$v_y^{(n)}(i,j)=v_y^{(n-2)}(i,j)+\frac{1}{\rho}\frac{\Delta t}{\delta}\left[T_{xy}^{(n-1)}(i+1,j)-T_{xy}^{(n-1)}(i-1,j)+T_{yy}^{(n-1)}(i,j+1)-T_{yy}^{(n-1)}(i,j-1)\right] \tag{8}$$

Eqs.(4)~(8) are the FDTD expressions useful in acoustic field computation. For the sake of brevity, the discussion here is confined to 2D cases. In these equations, δ and Δt are the lattice spacing and time step respectively. i and j are spatial indices. n is a temporal index. In order to obtain an adequate accuracy, δ should usually be less than $\lambda/10$, and Δt less than $\delta/\sqrt{2}c$ where c is the sound speed[1]. In an elastic medium, the speed of longitudinal waves is used in choosing the value of Δt.

2 Fluid media

In a fluid, shear stress does not exist, namely, $\mu = 0$. Eqs.(4) and (5) become identical:

$$T^{(n)}(i,j)=T^{(n-2)}(i,j)+\lambda\frac{\Delta t}{\delta}\left[v_x^{(n-1)}(i+1,j)-v_x^{(n-1)}(i-1,j)+v_y^{(n-1)}(i,j+1)-v_y^{(n-1)}(i,j-1)\right] \tag{9}$$

Similarly, Eqs.(7) and (8) are simplified

$$v_x^{(n)}(i,j)=v_x^{(n-2)}(i,j)+\frac{1}{\rho}\frac{\Delta t}{\delta}\left[T^{(n-1)}(i+1,j)-T^{(n-1)}(i-1,j)\right] \tag{10}$$

$$v_y^{(n)}(i,j)=v_y^{(n-2)}(i,j)+\frac{1}{\rho}\frac{\Delta t}{\delta}\left[T^{(n-1)}(i,j+1)-T^{(n-1)}(i,j-1)\right] \tag{11}$$

And Eq.(6) is reduced to

$$T_{xy}^{(n)}(i,j) = T_{xy}^{(n-2)}(i,j) \tag{12}$$

Eq.(12) indicates that, if T_{xy} is zero initially, it will be zero for ever. In a fluid, $T = T_{xx} = T_{yy} = -p$. It is thus obvious that Eqs.(9)~(11) are identical to the basic expressions for fluid media given in [1], taking into account $\lambda = \rho c^2$.

3 Boundary conditions

Consider an incident sound wave in a fluid propagated toward a solid object. The normal components of both stress and particle displacement should be continuous across the boundary. The tangential stress component should also be continuous[10]. Since tangential stress is absent in the fluid, it should simply be set to zero on the boundary. Therefore the following boundary conditions result:

$$\left.\begin{aligned} T_{xx} &= T_{yy} = -p \\ T_{xy} &= 0 \\ v_x &= \alpha^2 u_x + \alpha\beta u_y \\ v_y &= \alpha\beta u_x + \beta^2 u_y \end{aligned}\right\} \tag{13}$$

where p is sound pressure in the liquid, u_x and u_y are velocity on the fluid side. α and β are direction cosines of the surface normal.

4 Unified FDTD formulae

The above expressions for fluids and elastic media may be modified to yield the following unified form:

$$T_{xx}^{(n)}(i,j) = T_{xx}^{(n-2)}(i,j) + \frac{1}{C_k}\frac{\Delta t}{\delta}\left[v_x^{(n-1)}(i+1,j) - v_x^{(n-1)}(i-1,j) + v_y^{(n-1)}(i,j+1) - v_y^{(n-1)}(i,j-1)\right] - \frac{2}{B_k}\frac{\Delta t}{\delta}\left[v_y^{(n-1)}(i,j+1) - v_y^{(n-1)}(i,j-1)\right] \tag{14}$$

$$T_{yy}^{(n)}(i,j) = T_{yy}^{(n-2)}(i,j) + \frac{1}{C_k}\frac{\Delta t}{\delta}\left[v_x^{(n-1)}(i+1,j) - v_x^{(n-1)}(i-1,j) + v_y^{(n-1)}(i,j+1) - v_y^{(n-1)}(i,j-1)\right] - \frac{2}{B_k}\frac{\Delta t}{\delta}\left[v_x^{(n-1)}(i+1,j) - v_x^{(n-1)}(i-1,j)\right] \tag{15}$$

$$T_{xy}^{(n)}(i,j) = T_{xy}^{(n-2)}(i,j) + \frac{1}{B_k}\frac{\Delta t}{\delta}\left[v_y^{(n-1)}(i+1,j) - v_y^{(n-1)}(i-1,j) + v_x^{(n-1)}(i,j+1) - v_x^{(n-1)}(i,j-1)\right] \tag{16}$$

$$v_x^{(n)}(i,j) = v_x^{(n-2)}(i,j) + \frac{1}{\rho_k}\frac{\Delta t}{\delta}\left[T_{xx}^{(n-1)}(i+1,j) - T_{xx}^{(n-1)}(i-1,j) + T_{xy}^{(n-1)}(i,j+1) - T_{xy}^{(n-1)}(i,j-1)\right] \tag{17}$$

$$v_y^{(n)}(i,j) = v_y^{(n-2)}(i,j) + \frac{1}{\rho_k}\frac{\Delta t}{\delta}\left[T_{xy}^{(n-1)}(i+1,j) - T_{xy}^{(n-1)}(i-1,j) + T_{yy}^{(n-1)}(i,j+1) - T_{yy}^{(n-1)}(i,j-1)\right] \tag{18}$$

In these equations, the subscript k may take a value 1 or 2, representing the fluid and the elastic object respectively. In each medium, C_k and B_k are compliance coefficients with respect to compressive strain and shear strain, respectively:

$$\left.\begin{aligned} C_k &= \frac{1}{\lambda_k + 2\mu_k} = \frac{1}{\rho_k c_k^2}, \qquad k = 1, 2 \\ B_k &= \frac{1}{\mu_k} = \frac{1}{\rho_k b_k^2}, \qquad k = 1, 2 \end{aligned}\right\} \tag{19}$$

where c_k and b_k are velocities of the longitudinal and transverse waves respectively.

In the fluid, $B_1 = \infty$ because $\mu_1 = 0$, whereas on the boundary, average values of the compliance coefficients and the densities on both sides are used:

$$C_{12} = \frac{1}{2}\left(C_1 + C_2\right) = \frac{\rho_1 c_1^2 + \lambda + 2\mu}{2\rho_1 c_1^2\left(\lambda + 2\mu\right)} = \frac{\rho_1 c_1^2 + \rho_2 c_2^2}{2\rho_1 c_1^2 \rho_2 c_2^2} \tag{20}$$

$$B_{12} = \frac{1}{2}\left(B_1 + B_2\right) = \infty \tag{21}$$

$$\rho_{12} = \frac{1}{2}\left(\rho_1 + \rho_2\right) \tag{22}$$

It will be shown later in the numerical experiment section that this intuitive boundary treatment leads to results that conform with the boundary conditions given in Eq.(13).

III. Algorithm improvement

1 Motivations

It is clear from the preceding discussion that any FDTD field simulation may be implemented by a straightforward serial computation. The algorithm involves nested loops with three (in 2D cases) or four (in 3D cases) layers. The outermost layer is a temporal loop that does the primary iteration to mimic the wave propagation. In the inner loops, the sound field at each lattice node is calculated also in a serial fashion.

With the serial approach, FDTD is generally limited to low frequency applications with relatively small objects. For many practical problems, however, especially in 3D cases, the required computation time will be prohibitively long. Therefore, it is desirable to improve the algorithm by eliminating the inner loops and using a parallel structure instead.

The motivation for parallelism is threefold. First, it is directly related to the properties of the specific numerical tool used in the experiments. This matrix oriented programming language is much more efficient in doing matrix and array processing, which is parallel in nature, than executing loops. When using a general programming language such as c, a similar array operator may be defined so that the same algorithm can be implemented. Besides the other advantages to be explained below, parallelism at least simplifies the program structure.

Secondly, in most practical applications, it is necessary to spread the enormous computation burden among a group of parallel processors. This will be possible only when the serial calculation in the space domain is removed. FDTD by distributed parallel computing will be discussed in a separate publication as it is outside the scope of this paper.

Thirdly, in scattering problems, objects must be modeled. In other words, samples on the object boundary must be approximated to the nearest lattice nodes. Unfortunately, this seemingly simple task becomes quite involved if the scattering object has a complicated shape. Parallelism of the FDTD formulation will significantly ease the problem.

2 FDTD formulae in a form of array operation

From the observation of Eqs.(14)~(17), simultaneous array operations in the space domain may be realized by introducing the following set of two dimensional arrays:

$\mathbf{v}_{x,E}$, where $v_{x,E}(i, j) = v_x(i + 1, j)$

$\mathbf{v}_{x,W}$, where $v_{x,W}(i, j) = v_x(i - 1, j)$

$\mathbf{v}_{x,N}$, where $v_{x,N}(i, j) = v_x(i, j + 1)$

$\mathbf{v}_{x,S}$, where $v_{x,S}(i, j) = v_x(i, j - 1)$

$\mathbf{v}_{y,E}$, where $v_{y,E}(i, j) = v_y(i + 1, j)$

$\mathbf{v}_{y,W}$, where $v_{y,W}(i, j) = v_y(i - 1, j)$

$\mathbf{v}_{y,N}$, where $v_{y,N}(i, j) = v_y(i, j + 1)$

$\mathbf{v}_{y,S}$, where $v_{y,S}(i, j) = v_y(i, j - 1)$

These are shifted versions of the original arrays $\mathbf{v}_x$ and $\mathbf{v}_y$, all sized $(M-2) \times (N-2)$ where M and N are the numbers of lattice nodes in both coordinates. The letters in the subscripts after a comma stand for east, west, north, and south, respectively. Shifted arrays $\mathbf{T}_{xx,E}$, $\mathbf{T}_{xy,S}$, etc., can also be defined for the stress components in the same way. All the original and shifted arrays are thus in alignment spatially as shown in Fig.1.

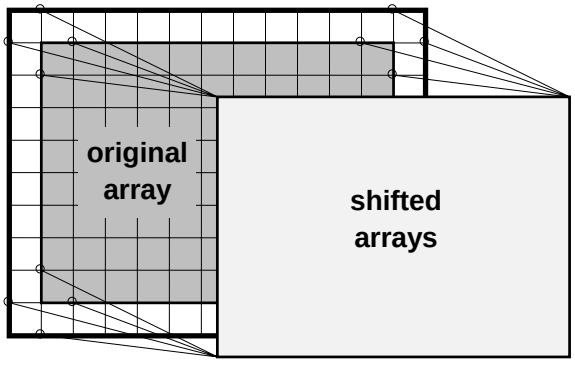

Fig.1 Alignment of shifted arrays

Also, the following arrays are defined for the material-related multiplicative constants:

$$\mathbf{G} = \frac{\Delta t}{\delta}\left[\frac{1}{C_1}\mathbf{W} + \frac{1}{C_2}\mathbf{O} + \frac{1}{C_{12}}\mathbf{X}\right] \tag{23}$$

$$\mathbf{F} = \frac{\Delta t}{\delta}\left[\frac{1}{B_1}\mathbf{W} + \frac{1}{B_2}\mathbf{O} + \frac{1}{B_{12}}\mathbf{X}\right] \tag{24}$$

$$\mathbf{H} = \frac{\Delta t}{\delta}\left[\frac{1}{\rho_1}\mathbf{W} + \frac{1}{\rho_2}\mathbf{O} + \frac{1}{\rho_{12}}\mathbf{X}\right] \tag{25}$$

W, **O**, and **X** are termed *shape arrays* corresponding to water, object, and boundary respectively. They have the same size with the velocity and stress arrays. In **W**, all elements corresponding to the lattice nodes in the water equal to unit, and the others are zero. Similarly, all elements in **O** corresponding to the nodes inside the scattering object equal to unit and the others are zero, while in **X**, all boundary nodes are unit, and the rest are zero.

With all these array symbols defined, Eqs.(14)~(18) can be rewritten in a compact form:

$$\mathbf{T}_{xx}^{(n)} = \mathbf{T}_{xx}^{(n-2)} + \mathbf{G} \bullet \left[\mathbf{v}_{x,E}^{(n-1)} - \mathbf{v}_{x,W}^{(n-1)} + \mathbf{v}_{y,N}^{(n-1)} - \mathbf{v}_{y,S}^{(n-1)}\right] - 2\mathbf{F} \bullet \left[\mathbf{v}_{y,N}^{(n-1)} - \mathbf{v}_{y,S}^{(n-1)}\right] \tag{26}$$

$$\mathbf{T}_{yy}^{(n)} = \mathbf{T}_{yy}^{(n-2)} + \mathbf{G} \bullet \left[\mathbf{v}_{x,E}^{(n-1)} - \mathbf{v}_{x,W}^{(n-1)} + \mathbf{v}_{y,N}^{(n-1)} - \mathbf{v}_{y,S}^{(n-1)}\right] - 2\mathbf{F} \bullet \left[\mathbf{v}_{x,E}^{(n-1)} - \mathbf{v}_{x,W}^{(n-1)}\right] \tag{27}$$

$$\mathbf{T}_{xy}^{(n)} = \mathbf{T}_{xy}^{(n-2)} + \mathbf{F} \bullet \left[\mathbf{v}_{y,E}^{(n-1)} - \mathbf{v}_{y,W}^{(n-1)} + \mathbf{v}_{x,N}^{(n-1)} - \mathbf{v}_{x,S}^{(n-1)}\right] \tag{28}$$

$$\mathbf{v}_{x}^{(n)} = \mathbf{v}_{x}^{(n-2)} + \mathbf{H} \bullet \left[\mathbf{T}_{xx,E}^{(n-1)} - \mathbf{T}_{xx,W}^{(n-1)} + \mathbf{T}_{xy,N}^{(n-1)} - \mathbf{T}_{xy,S}^{(n-1)}\right] \tag{29}$$

$$\mathbf{v}_{y}^{(n)} = \mathbf{v}_{y}^{(n-2)} + \mathbf{H} \bullet \left[\mathbf{T}_{xy,E}^{(n-1)} - \mathbf{T}_{xy,W}^{(n-1)} + \mathbf{T}_{yy,N}^{(n-1)} - \mathbf{T}_{yy,S}^{(n-1)}\right] \tag{30}$$

In these equations, the thick dot sign is an array operator, taking element-wise multiplication between two arrays and resulting in a new array of the same size. These equations are used in calculation of the sound field inside the computation domain shown as the gray area in Fig.1. The field on the truncating boundary illustrated by a thick frame outside the gray region in the figure is calculated from the absorbing boundary conditions[2].

3 Modeling complicated shaped objects

It should be pointed out that, in a serial algorithm, modeling a complicated shaped target is not a trivial task. This is partly because an object having a complicated shape is usually difficult to describe using a simple analytical geometry equation. Besides, the discretized boundary points must be arranged in a known order so that they can easily be identified in the execution of the spatial loops.

It is clear from Eqs.(26)~(30) that the order of the boundary points is no longer important in an array operation. This makes it possible to model a complicated object by simply decomposing it into several elementary shapes. Consider a target composed of a circle and a rectangle, as shown in Fig.2. Each elementary shape has three shape arrays, $\mathbf{W}_i$, $\mathbf{O}_i$, and $\mathbf{X}_i$, where i = 1, 2. The composite shape-arrays may be obtained from

$$\left.\begin{aligned} \mathbf{X} &= (\mathbf{X}_1 \bigcup \mathbf{X}_2) - (\mathbf{X}_1 \bigcap \mathbf{O}_2) - (\mathbf{X}_2 \bigcap \mathbf{O}_1) \\ \mathbf{O} &= \mathbf{O}_1 \bigcup \mathbf{O}_2 \\ \mathbf{W} &= \mathbf{E} - (\mathbf{O} + \mathbf{X}) \end{aligned}\right\} \tag{31}$$

where **E** is an array with all elements equal to unit. In Eq.(31), boundary points belonging to one object and falling into another, shown as the white circles in Fig.2, become interior nodes, therefore are excluded from **X**. The special cases in which two objects are mutually tangent is not considered here.

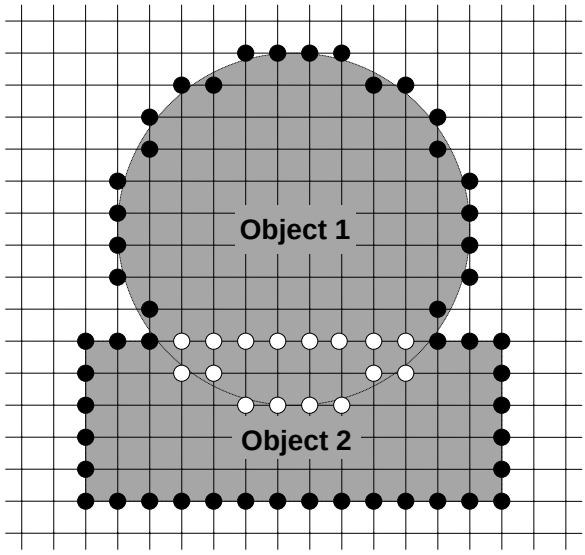

Fig.2 A target made of two elementary objects

IV. Numerical Results

In the numerical experiments, an aluminum target composed of a rectangular cylinder and a circular cylinder was used. The circular cylinder had a radius 1.6 m. The principal section of the rectangular cylinder was measured 1.4 m × 4.5 m with the longer side forming a 30° angle with the horizontal axis. The densities and the elastic constants of the media used in the computation were:

$\rho_1 = 1026$ kg/m^3, $c_1 = 1500$ m/s,

$\rho_2 = 2700$ kg/m^3, $E_2 = 7.1 \times 10^{10}$ Newton/m^2, and $\sigma_2 = 0.33$,

where E_2 and σ_2 are Young's modulus and Poisson's ratio, respectively, from which the Lame constants can be derived:

$$\lambda = \frac{E\sigma}{(1+\sigma)(1-2\sigma)} \tag{32}$$

$$\mu = \frac{E}{2(1+\sigma)} \tag{33}$$

The incident plane wave was sinusoidal, having a frequency 1500 Hz. The finite-difference

parameters used in the computation were $\delta = \lambda_1 /15$, and $\Delta t = \delta /2c_2$.

The field patterns obtained by using the improved algorithm are presented in Fig.3, where Figs.3(a)~(c) are the instantaneous distributions of $\mathbf{T}_{xx}$, $\mathbf{T}_{yy}$, and $\mathbf{T}_{xy}$, respectively, Fig.3(d) is the scattered sound pressure with the incident wave subtracted, and Figs.3(e) and (f) are the velocity components $\mathbf{v}_x$ and $\mathbf{v}_y$ respectively. No plane wave contents can be found in $\mathbf{v}_y$, as $\mathbf{v}_y$ simply does not exist in the incident wave, and is entirely induced by the scattering object. It is observed that $\mathbf{T}_{xx}$ and $\mathbf{T}_{yy}$ are identical in the water, equal in magnitude to sound pressure, p, with a sign reversal. The shear stress $\mathbf{T}_{xy}$ exists only within the steel target, and vanishes towards its surface as more clearly shown in Fig.4 below.

Field distribution patterns may as well be obtained by using a serial algorithm. Both the serial and the improved algorithms give the same results. However, the computing time required by the former was more than 10 times as much as required in the present work using the improved method.

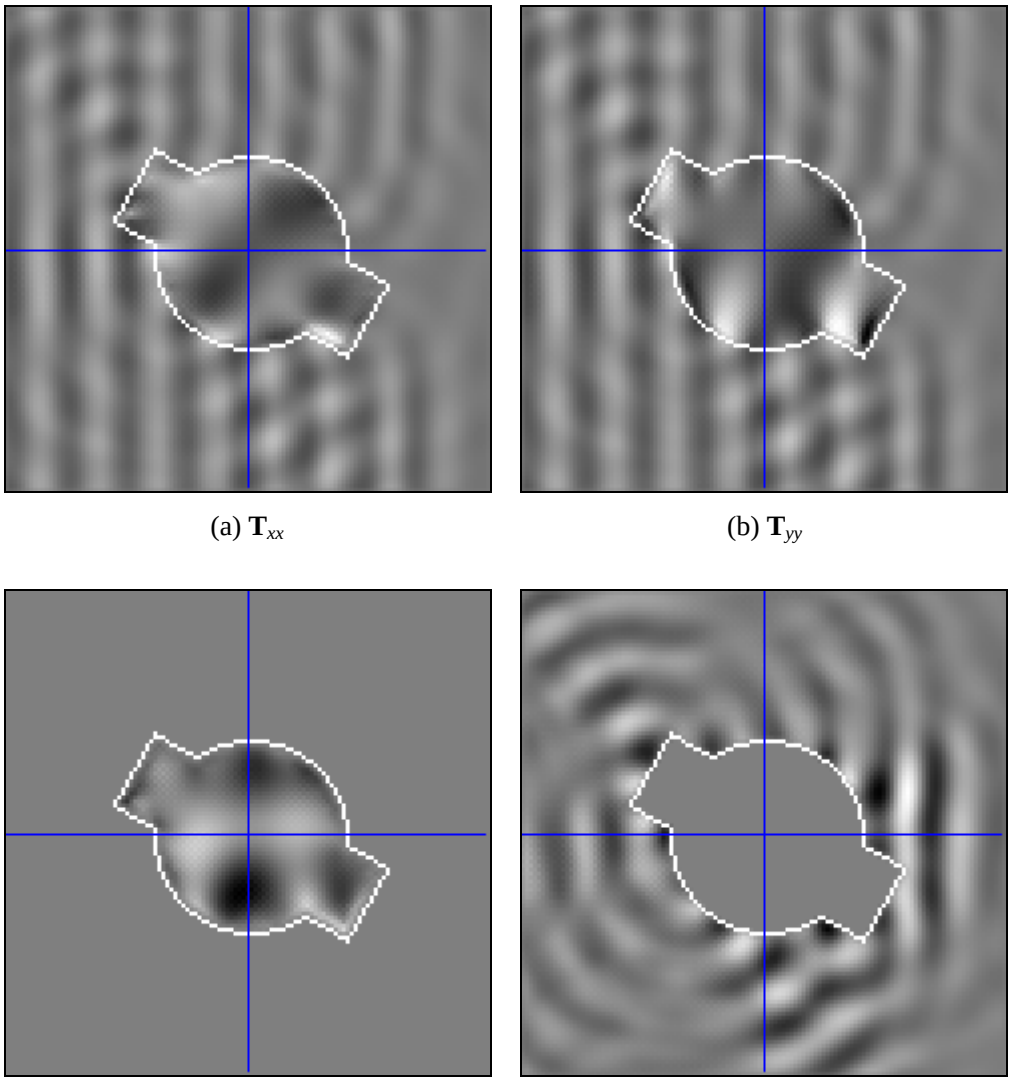

(a) $\mathbf{T}_{xx}$ (b) $\mathbf{T}_{yy}$

(c) $\mathbf{T}_{xy}$ (d) $\mathbf{P}_{\text{scat}}$

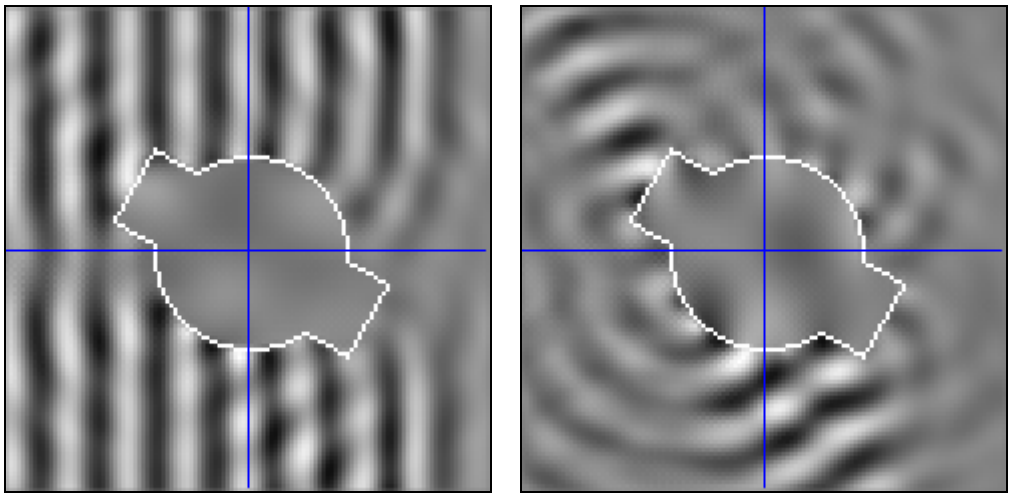

(e) $\mathbf{v}_x$ (f) $\mathbf{v}_y$

Fig.3 Acoustic field distribution around the composite aluminum target

The boundary conditions described by Eq.(13) may be checked from the curves given in Figs.4~6. Fig.4 presents the distribution of $\mathbf{T}_{xx}$, $\mathbf{T}_{yy}$, and $\mathbf{T}_{xy}$ along the middle horizontal line. The two vertical dash-dotted lines indicate the boundary locations. It is clear that both $\mathbf{T}_{xx}$ and $\mathbf{T}_{yy}$ are continuous across the boundary, and $\mathbf{T}_{xy}$ is zero at the boundary as well as outside the scattering object.

Fig.5 gives the particle velocity distribution along the middle horizontal line. Note that the normal velocity v_x is continuous at the boundary where the directional cosine of the surface normal $\beta = 0$, whereas the tangential velocity v_y may have jumps across the boundary. Similarly, Fig.6 gives the particle velocity distribution along the center vertical line. The normal velocity v_y is continuous at the boundary where the directional cosine $\alpha = 0$, whereas the tangential velocity v_x may have jumps across the boundary. In this example, v_x does show significant jumps at both horizontal interfaces.

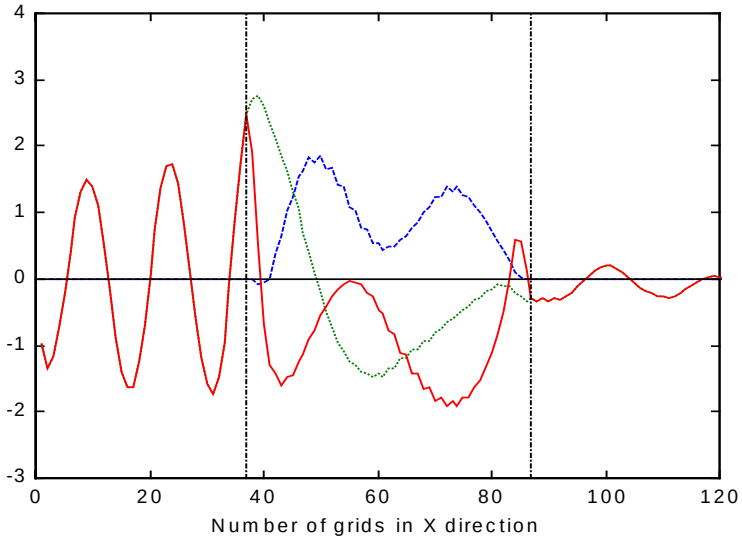

Fig.4 Stress components along the middle horizontal line.

Solid: T_{xx}, Dotted: T_{yy}, Dashed: T_{xy}

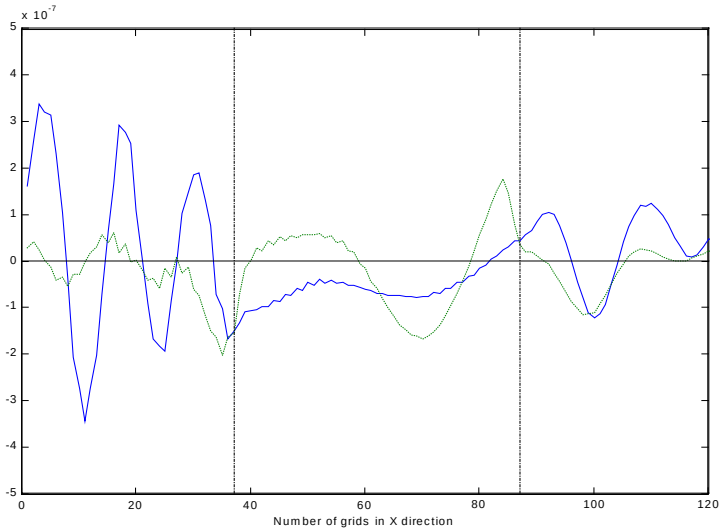

Fig. 5 Velocity components along the middle horizontal line.

Solid: v_x, Dotted: v_y

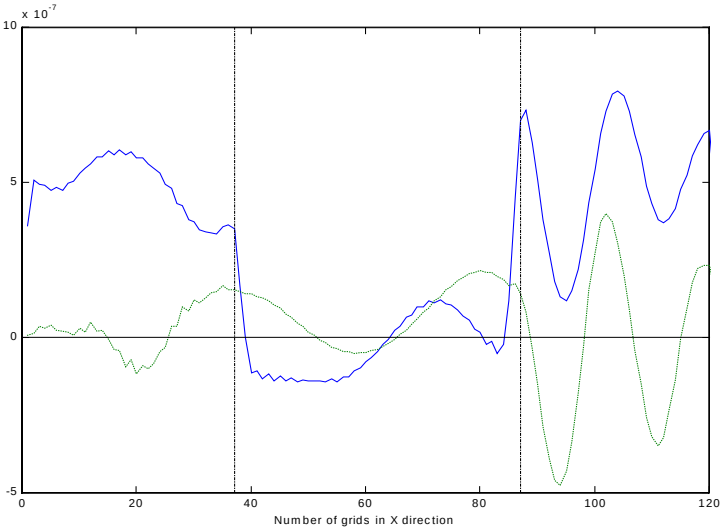

Fig. 6 Velocity components along the center vertical line.

Solid: v_x, Dotted: v_y

Fig.7 gives the far field directional patterns of the circular cylinder, the rectangular cylinder, and the combined target, respectively. These patterns are computed from the near field distributions using a discrete Fourier transform method[1]. In the case of a rectangular cylinder, there are two major lobes corresponding to specular reflections from the two flat surfaces. In the composite target case, the lobe at 120° is basically retained as the narrower side of the rectangular cylinder is still exposed to the incident wave. On the other hand, the otherwise biggest lobe at 300° is reduced, and several other peaks are also modified, due to the introduction of the circular cylinder.

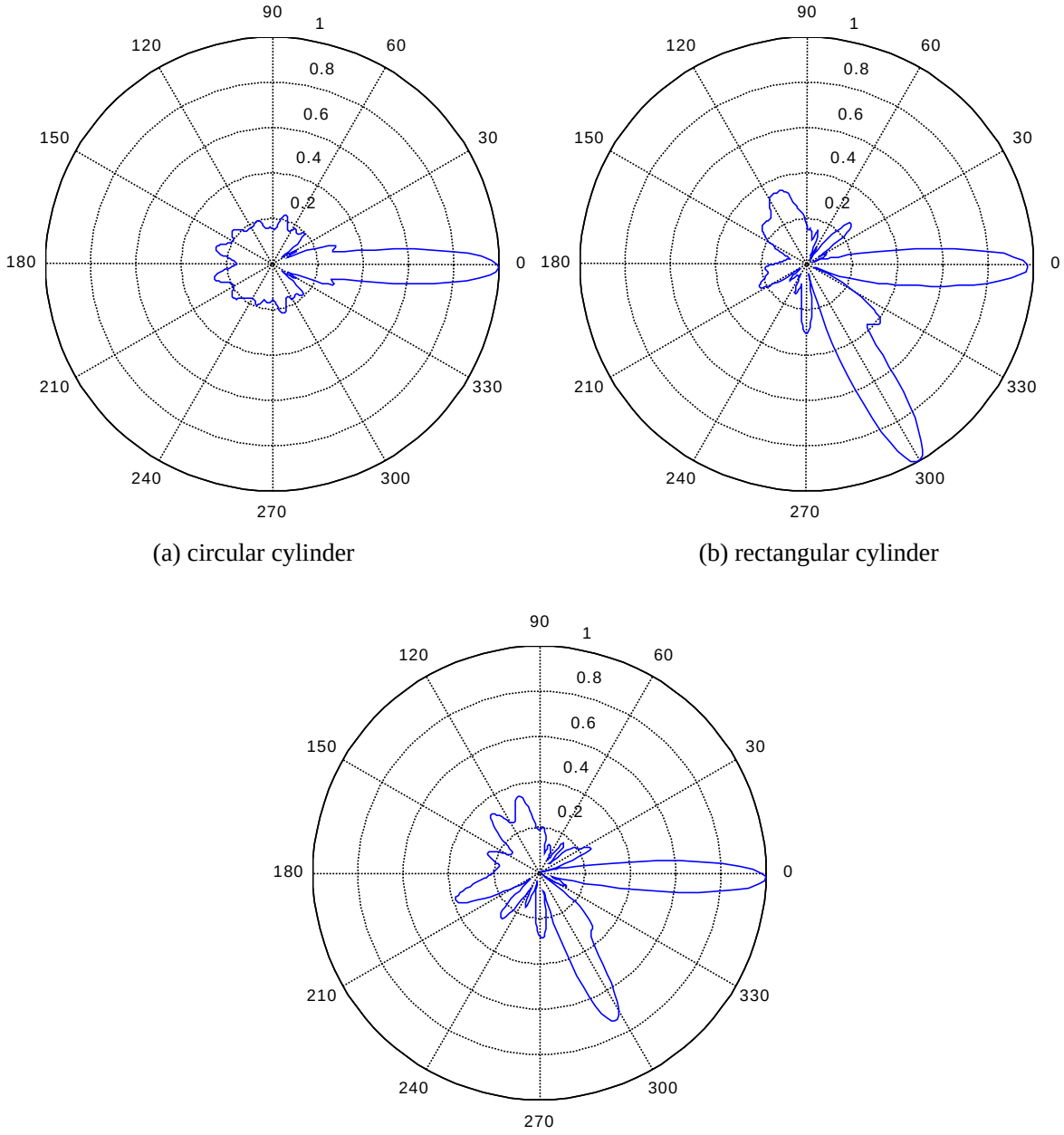

(a) circular cylinder

(b) rectangular cylinder

(c) composite target

Fig.7 Far field directional patterns

V. Conclusions

A set of unified FDTD formulae have been presented, applicable to sound scattering from a wide range of objects, including liquids and elastic bodies supporting shear strains. With the prospective parallel computing for the finite-difference field simulation in mind, these formulae have been rewritten in a neater and more compact form. The new form leads to an improved algorithm in which most loops for the space domain evaluation are eliminated and replaced by simultaneous array operations.

Programs based on the improved algorithm are much more efficient than the previous method when implemented using array and matrix oriented programming languages. Also, complicated target shapes can easily be modeled by decomposing them into several elementary objects. Numerical experiments using the new algorithm have been carried out. The results have shown to conform with the boundary conditions, as well as with the field distributions obtained by the serial approach.

An important merit of the new algorithm is to provide a basis for the distributed parallel computing. This is currently under intensive investigation in order to expand the FDTD field modeling to more practical applications.

References

[1] Wang S, "Finite-Difference Time-Domain Approach to Underwater Acoustic Scattering Problems," *J. Acoust. Soc. Am.*, **99**(4), pt.1, 1996: 1924–1931

[2] Wang S, "An Efficient Absorbing Boundary for Finite-Difference Time-Domain Field Modeling in Acoustics," *Chin. J. Acoust.*, **16**(2), 1997: 121–134

[3] Liu Q H, Schoen E, Daube F, Rabdall C, Liu H, and Lee P, "A Three-Dimensional Finite-Difference Simulation of Sonic Logging," *J. Acoust. Soc. Am.*, **100**(1), 1996: 72–79

[4] Stephen R A, "Modeling Sea Surface Scattering by Time-Domain Finite-Difference Method,' *J. Acoust. Soc. Am.*, **100**, 1996: 2070–2078

[5] Hastings F D, Schneider J B, and Broschat S L, "A Finite-Difference Time-Domain Solution to Scattering from a Rough Pressure-Release Surface," *J. Acoust. Soc. Am.*, **102**(6), 1997: 3394–3400

[6] Schneider J B, Wagner C L, and Broschat S L, "Implementation of Transparent Sources Embedded in Acoustic Finite-Difference Time-Domain Grids," *J. Acoust. Soc. Am.*, **103**(1), 1998: 136–142

[7] Wang S, Wang T, and Wang R, "FDTD Boundary Treatment for Scattering from Penetrable Objects," *J. Acoust. Soc. Am.*, **102**(11), pt.2, 1997: 3088

[8] Wang S, and Wang T, "Computation of Sound Scattering from Penetrable Objects Using Finite-Difference Time-Domain Method," *Tech. Acoust.*, 17(1), 1998: 2–5 (in Chinese)

[9] Wang S, "Unified FDTD Expressions for Sound Scattering by Elastic Objects," *Academic Periodical Abstracts of China*, 4(4), 1998: 477–479 (in Chinese)

[10] Brekhovskikh L, *Waves in Layered Media*, Academic Press, 1960: Section 4